# A Radial Standing Pc5-6 Wave and its Energy Coupling with Field Line Resonance within the Dusk-sector Magnetosphere

Yi-Jia Zhou[1,2], Fei He[1,2*], Xiao-Xin Zhang[3], Martin O. Archer[4], Yu Lin[5], Han Ma[1,2], An-Min Tian[6], Zhong-Hua Yao[1,2], Yong Wei[1,2], Binbin Ni[7], Wenlong Liu[8], Qiu-Gang Zong[9], Zu-Yin Pu[9]

[1]Key Laboratory of Earth and Planetary Physics, Institute of Geology and Geophysics, Chinese Academy of Sciences, Beijing 100029, China.

[2]Colleage of Earth and Planetary Science, University of Chinese Academy of Sciences, Beijing 100049, China.

[3]Key Laboratory of Space Weather, National Center for Space Weather, China Meteorological Administration, Beijing 100081, China.

[4]Space and Atmospheric Physics Group, Department of Physics, Imperial College London, London, UK.

[5]Physics Department, Auburn University, Auburn, Alabama, USA

[6]School of Space Science and Physics, Shandong University, Weihai 264209, China.

[7]Department of Space Physics, School of Electronic Information, Wuhan University, Wuhan 430072, China

[8]School of Space and Environment, Beihang University, Beijing 100191, China.

[9]Institute of Space Physics and Applied Technology, Peking University, Beijing 100871, China.

*Corresponding author: Fei He (hefei@mail.iggcas.ac.cn)

**Key Points:**

1. A radial standing Pc5-6 ULF wave is identified within the dusk-sector magnetosphere.
2. Radial standing wave dissipates energy into upper atmosphere by coupling itself to the FLR.
3. Solar-wind and/or magnetosheath dynamic pressure/velocity fluctuations possibly trigger this radial standing wave.

## Abstract

Global ultra-low frequency (ULF) oscillations are believed to play a significant role in the mass, energy, and momentum transport within the Earth's magnetosphere. In this letter, we observe a ~1.2 mHz radial standing wave in the dusk-sector magnetosphere accompanied by the field line resonance (FLR) on 16 July 2017. The frequency estimation from the simple box model also confirms the radial standing wave. The essential characteristics of FLR are concurrently identified at the dusk-sector magnetosphere and the conjugated ground location. Further, the radial standing wave dissipates energy into upper atmosphere to enhance the local aurora by coupling itself to the FLR. The magnetospheric dominant 1.2/1.1 mHz ULF waves plausibly correspond well with the discrete ~1 mHz magnetosheath ion dynamic pressure/velocity oscillation, suggesting this radial standing wave and FLR in the flank magnetosphere may be triggered by the solar-wind and/or magnetosheath dynamic pressure/velocity fluctuations.

## Plain Language Summary

Just like thumping the strings, the Earth's magnetic field line can also be disturbed by the external impulses or internal instability, generating the rich ultra-low frequency oscillations with period of 1-1000s. They are believed to play a significant role in the mass, energy, and momentum transport within the Earth's magnetosphere. But the question of how an external driving mechanism can produce field line disturbances deep inside the magnetosphere is a topic of much debate. One classical global mode resonance model suggests that the magnetospheric space sometimes acts as a huge closed or semi-closed cavity, where the ultra low frequency waves form the radial standing wave structure. So far, the observational evidence of radial standing waves with period of above 8 minutes accompanied by the field line disturbance in the flank magnetosphere is sparse. In this letter, we report a radial standing wave with period of ~14 minutes within dusk-sector magnetosphere accompanied by the field line disturbance phenomenon by multiple-satellite observations. The radial standing wave energy sinks down to upper atmosphere to light the local aurora by coupling itself to the field line resonance. We conclude the radial standing wave may be caused by the solar-wind and/or magnetosheath dynamic pressure/velocity fluctuations.

**Keywords:** Ultra-Low Frequency (ULF) Wave, Standing Wave, Field Line Resonance (FLR), Magnetosheath Fluctuation

## 1. Introduction

Boundaries in the terrestrial magnetosphere, such as the magnetopause (MP; e.g., Lin et al., 2010) and the plasmapause (PP; e.g., Zhang et al., 2017; He et al., 2017), are of primary importance in controlling the flow of mass, energy and momentum from the solar wind into the terrestrial space environment. Their motion can have direct and indirect space weather impacts on the radiation belts, auroral oval and ionosphere (e.g., Summers et al., 2013; Elkington, 2006; Keiling et al., 2016). A large part of the magnetospheric electromagnetic energy is carried and regulated by ultra-low frequency (ULF) waves that coupling different regions together. The magnetospheric ULF wave can be driven externally by solar wind perturbation including dynamic pressure impulse/shock (e.g., Allan et al., 1986; Mann et al., 1998; Takahashi et al., 2018) and periodic fluctuations (e.g., Kepko & Spence, 2003; Stephenson & Walker, 2002; Motoba et al., 2003; Fenrich & Waters, 2008; Di Matteo et al., 2022), ion foreshock transient phenomena (e.g., Hartinger et al., 2013a; Wang, B. et al., 2020), subsolar MP surface wave (e.g., Archer et al., 2019) and flank Kelvin-Helmholtz (K-H) waves (e.g., Pu et al., 1983; Mann et al., 1999, 2002; Wright et al., 2000; Rae et al., 2005, Agapitov et al., 2009), or internally by, for instance, plasma instabilities in the nightside and dayside magnetosphere (e.g., Keiling, 2009; Glassmeier et al., 1999; Yamakawa et al., 2022), but with no consensus on the dominant one.

One of the paradigms of ULF pulsation theory is the resonant coupling of a compressional surface wave with toroidal oscillations somewhere deeper in the magnetosphere. Compressional waveguide modes, excited by the K-H instability, can also couple to a field line resonance (FLR) (Mann et al., 1999; Mills & Wright, 1999). Specifically, these compressional modes, spatially decaying toward the inner magnetosphere, can couple to the shear Alfvén waves at discrete L-shells, where the eigenfrequency of local magnetic field line matches the frequency of driving surface wave, resulting in the classical FLR (Southwood, 1974). Theoretically, the toroidal FLR is identified by a ~180° phase shift in the toroidal perturbations or the polarization reversal across the amplitude maximum (e.g., Agapitov et al., 2009; Nishida, 2013) in space and similar ground signatures of the geomagnetic field H component (e.g., Samson et al., 1971; Rae et al., 2005). Through the FLR mechanism, compressional wave energy can be efficiently transferred to shear Alfvén waves and subsequently be deposited down to the ionosphere via energetic auroral particles and Joule heating (e.g., Kivelson & Southwood, 1986; Rae et al., 2007; Hartinger et al., 2011; Golovchanskaya et al., 2018).

To rationalize observations of the nearly monochromatic ULF wave activity over a range of L shells, the cavity modes resonance (CMR) model was first postulated and applied to near the subsolar region, where the compressional mode energy with harmonic frequencies can be trapped between the MP and the reflection region inside the magnetosphere (e.g., Kivelson et al., 1984; Zhu & Kivelson, 1989; Lee & Lysak, 1989; Kivelson et al., 1997; Samson et al., 1992a; Mann et al., 1995; Keiling et al., 2001;

Claudepierre et al., 2009; Takahashi et al., 2010, 2018). While the flank magnetosphere is regarded as an open-ended waveguide, that is Waveguide Mode Resonance (WMR), to account for the energy loss through azimuthal/tail-ward transporting energy flows (e.g., Samson et al., 1992a,b; Mann et al., 2002; Rae et al., 2005; Eriksson et al., 2006; Elsden & Wright, 2019). The global mode resonance including CMR and WMR concerns radially standing fast magnetosonic waves, providing the frequency selection mechanism of magnetospheric and ground ULF waves. Notably, an azimuthally uniform waveguide without discrete eigenfrequencies (azimuthal wavenumber) can also excite discrete frequency FLR (Wright, 1994; Rickard & Wright, 1994). Their frequencies are chiefly controlled by the magnetosphere configuration and radial Alfvén velocity profile (e.g., Samson et al., 1992a; Walker et al., 1992; Archer et al., 2015, 2017).

Regardless of some evidences of global modes in the plasmasphere typically at frequencies above the Pc5 range (e.g., Takahashi et al., 2010) and the statistical analysis of global modes outside the plasmasphere with 2-20 mHz frequencies (Hartinger et al., 2013b), there have been few direct observations of radial standing waves below 2 mHz frequency accompanied by the FLR in the flank magnetosphere (Rae et al., 2005; Piersanti et al., 2022). Remarkably, the standing waves with 1-2 mHz frequency are typically assumed to be cavity modes/global mode (radial standing mode; e.g., Kivelson & Southwood, 1985; Samson et al., 1992a) or are explained by the newly confirmed MP and PP surface waves (poloidal standing mode; Archer et al., 2019; He et al., 2020), displaying an increasingly crucial role on the terrestrial energy transportation. Therefore, we report a ~1.2 mHz radial standing wave in the dusk-sector magnetosphere accompanied by the FLR phenomenon based on conjugated observations from THEMIS, DMSP satellites and IMAGE magnetometer array, trying to identify the essential characteristics and effect of such low frequency ULF waves in the solar wind-magnetosphere-ionosphere coupled system.

## 2. Event Observation

We use magnetospheric data from three of the THEMIS satellites, THA, THD and THE in the afternoon-dusk magnetosphere (Angelopoulos, 2008). Each satellite is equipped with a fluxgate magnetometer (FGM) (Auster et al., 2008), an electric field instrument (EFI) (Bonnell et al., 2008), and an electrostatic analyzer (ESA) (McFadden et al., 2008a, 2008b). The FGM measures the background magnetic field and its low frequency fluctuations (up to 64 Hz) with an accuracy of 0.01 nT. The EFI provides reliable electric field measurements in the spin-plane with the component along the spin axis obtained by assuming $\mathbf{E}\cdot\mathbf{B}=0$ when the normal of the spin plane is sufficiently far from the direction of the background magnetic field. The ESA measures the thermal particle distributions, from which moments are calculated onboard or later at ground (ion: 5eV-25keV, electron: 6eV-30keV). The auroral disk images are acquired in $N_2$ Lyman-Birge-Hopfield (LBH) band from the SSUSI (Paxton et al., 2002) onboard DMSP satellites, and the geomagnetic field data (10 s resolution) originates from the IMAGE magnetometer array (Tanskanen, 2009). Due to the partial absence of OMNI solar wind data during this interval, we use the OMNIWeb 1-minute solar wind data that has been time-shifted to the Earth's Bow Shock Nose (BSN) based only on the Wind 3DP plasma data (Lin et al., 1995).

### 2.1 Solar Wind and Magnetosheath Conditions

Figure 1 displays the solar wind conditions including the main phase of a moderate geomagnetic storm and the trajectories of THA, THE and THD on 16 July 2017. The magnetospheric ULF wave event is captured within the dusk-sector magnetosphere at 11:30-15:00 UT, during which the IMF Bz/By is generally southward/eastward. The IMF Bz suddenly drops to below -20 nT at ~11:00 UT, rapidly recovers to ~0 nT at 13:00 UT, and sequentially slowly shifts towards -10 nT at about 14:00 UT. The solar wind speed exceeds over 500 km/s in Figure 1c. Just before this period, turbulent variations of IMF By and Bz components occurred, and the solar wind dynamic pressure reached peaks attributed to the enhanced proton density and solar wind velocity. Combined with the greatly enhanced *SYM-H* value (Storm Sudden Commencement, i.e., SSC; ~80 nT) followed by an abrupt decreasing to -65 nT and the intensified aurora electrojet (AE) shown in Figure 1e-1f, we can infer this geomagnetic storm is triggered by a corotating interaction region (CIR) event.

As shown in Figure 1g, during the period of 9:00-15:00 UT, THA and THE simultaneously travelled radially and azimuthally inward from the magnetosheath to inner magnetosphere near the magnetic equator, while THD entered the magnetosphere nearly two hours later. Note that THA and THE simultaneously arrived at locations with the nearly same L-shell but with a 0.8-hour MLT difference. Along the satellites' trajectories, the observed magnetosheath (9:30-11:00 UT for THA/E and 9:30-13:00 UT for THD), MP (11:15 for THA, 11:00 for THE and 13:15 for THD) and magnetospheric parameters (11:30-15:00 UT for THA/E) are individually demonstrated below in Figure 2 and Figure 3 in detail.

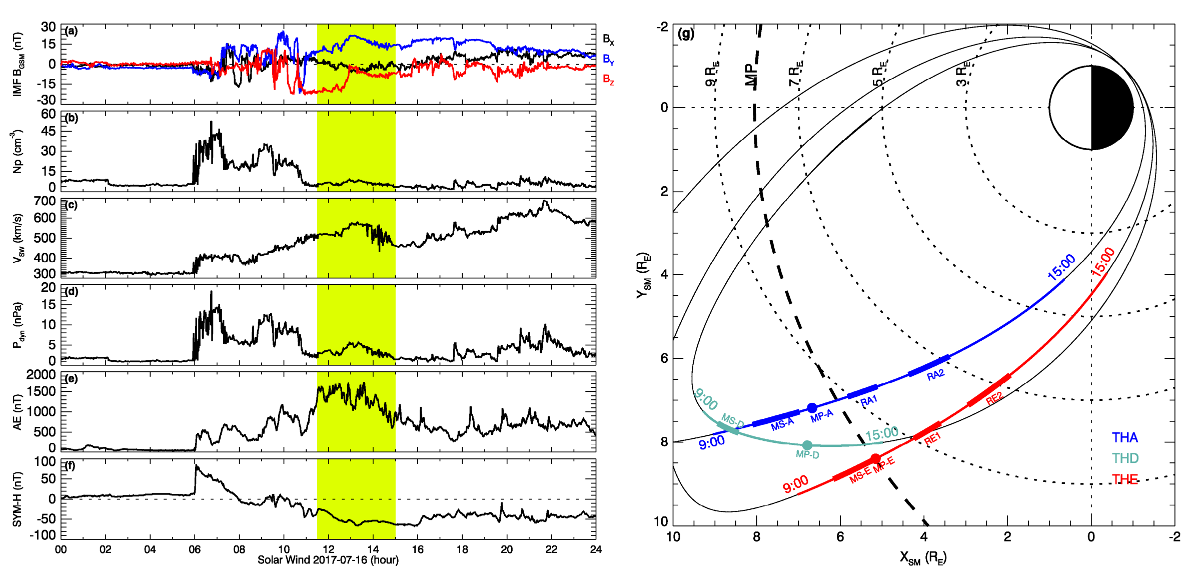

**Figure 1. Solar wind and satellites' trajectory on 16 July 2017**. (a-d) three components of IMF, solar wind proton density, velocity, and dynamic pressure; (e-f) *AE* and *SYM-H* indices; (g) trajectories of THA, THE and THD projected on the SM equator plane. The interval of magnetospheric ULF-wave is highlighted by the yellow shaded rectangle in Figures 1a-1f. The three dots denote the MP crossings by the three satellites. The regions of magnetosheath fluctuations are marked as MS-A, MS-D, and MS-E, respectively. The radial standing waves in the magnetosphere are marked as RA1 and RA2 for THA, and RE1 and RE2 for THE, respectively. The thick dashed curve represents the location of the MP under the averaged IMF and solar wind conditions between 11:00 and 12:00 UT as calculated with the Shue et al. (1998) model.

Figures 2a, 2c and 2e depict the quasi-periodic fluctuation of magnetic field, ions number density, velocity and dynamic pressure in the magnetosheath just outside the identified MP (vertical dashed lines). Correspondingly, utilizing a Morlet wavelet function to calculate their continuous power spectra density in Figures 2b, 2d and 2f, we can obtain that a dominant ~1 mHz frequency of the magnetosheath ion number density/dynamic pressure oscillation was detected synchronously by THA, THE and THD mainly at 10:00-11:00 UT (i.e., MS-A, MS-E, MS-D; gray shaded regions). During this period, the 7-min lagged (from the BSN to the MP) proton density and dynamic pressure of solar wind (black curves) demonstrate the nearly same fluctuation, suggesting the magnetosheath oscillation may originate from the solar wind. And this standpoint can also be supported by the evident 1-2 mHz frequency embedded in the solar wind parameters, especially the solar wind proton density, from wavelet power spectra in Figure S1. Based on Figure S1, after 11:00 UT, the above solar wind strength decreased rapidly but their inherent fluctuations persist, especially at 12:15-13:30 UT. Meanwhile, THA and THE plunged into the magnetosphere and THD continued to monitor the magnetosheath environment. During 11:30-13:30 UT, the similar ~1 mHz frequency is primarily reflected in the magnetosheath ion velocity oscillation, but is nearly invisible in the ion dynamic pressure mostly due to the rapidly decreasing ion number density.

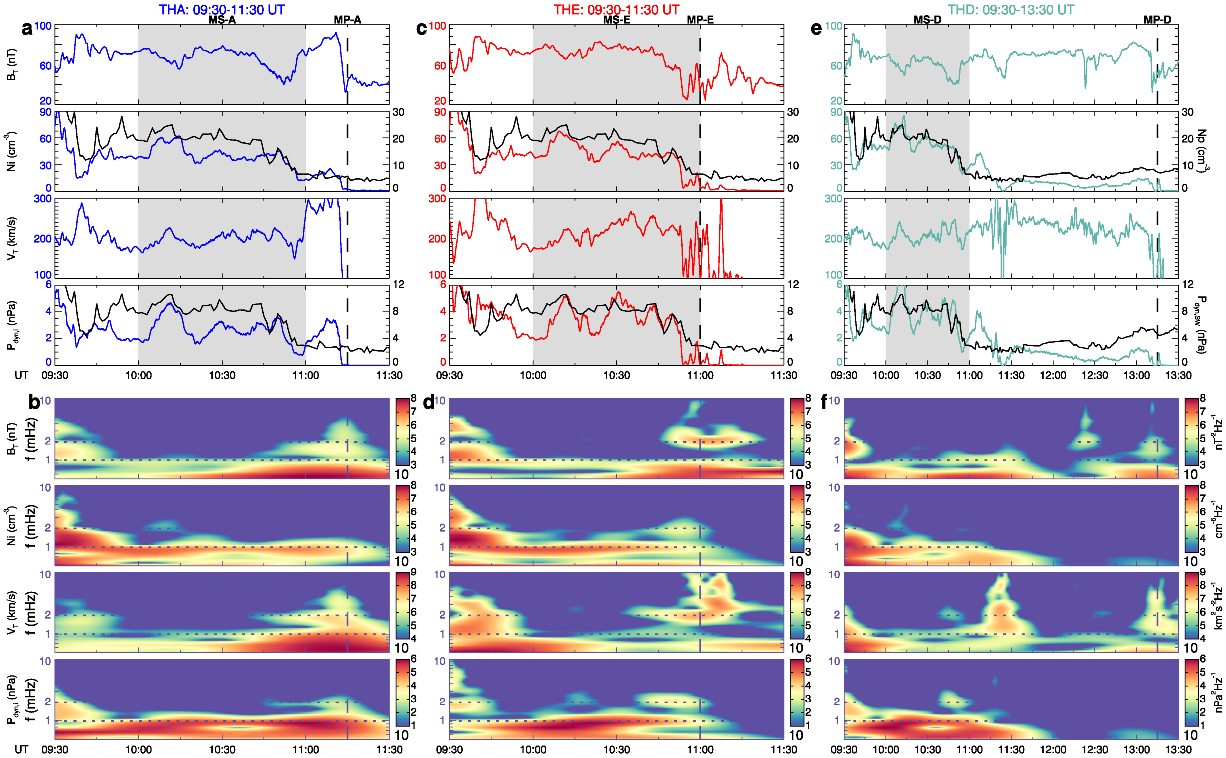


**Figure 2. Magnetosheath conditions observed by THA (first column), THE (second column) and THD (third column)**. (a) From top to bottom shown are magnetic field, ions number density, velocity, dynamic pressure observed by THA. (b) Morlet wavelet power spectra densities corresponding to the panels in (a); (c-d) similar arrangement as panels a-b but for THE; and (e-f) similar arrangement as panels a-b but for THD. The lagged proton density and dynamic pressure of solar wind (black curves) are also added to panels (a), (c) and (e). The intervals of magnetosheath fluctuation are highlighted by the gray shaded rectangles (MS-A/E/D) and the vertical dashed lines demark the MP crossings (MP-A/E/D). The 1 mHz and 2 mHz frequencies are marked by horizontal dotted lines.

## 2.2 Magnetosphere Observation

In Figure 3, the ULF wave is analyzed in the field-aligned (FA) coordinate system, in which $\mathbf{e}_p$ is along the background magnetic field (direction obtained from the 45-min sliding averaged data), $\mathbf{e}_a$ (roughly eastward) is parallel to $\mathbf{e}_p \times \mathbf{R}$ ($\mathbf{R}$ is the radial vector pointing from the center of the Earth toward the satellite), and $\mathbf{e}_r$ (roughly radially outward) completes the orthogonal set. To emphasize the field perturbation, the 45 min smooth-averaged field (background field) was subtracted to detrend the raw data, as shown in Figures 3f-3g and 4f-4g. We firstly calculate the power spectra of the magnetospheric magnetic and electric field perturbations in the FA coordinate during the interval of 11:30-15:00 UT. Evident power peaks appear at harmonic frequencies, including ~1.2, 2 and 3 mHz for THA in Figures 3a-3e, plausibly consistent with the discrete ~1 mHz oscillations of the solar wind and magnetosheath ion dynamic pressure. Note the different y/power axes scales for different field components. More directly from Figure 3f, we can obtain the detected ULF wave is dominated by the compressional components (Bp and Br) rather than the transversal waves (Ba). In Figures 3h, the total magnetic field fluctuates nearly in phase with the ion density, indicating the dusk-sector magnetosphere is undergoing the radial compression and expansion (Kivelson et al., 1984).

Centered at the most evident ~1.2 mHz frequencies, the bandpass of 0.8-1.5 mHz for THA is utilized to filter the raw field disturbances. Figures 3i-3j show that Bp and Ba intensify simultaneously (gray shaded region), roughly labeled as RA1 (11:54-12:24 UT) and RA2 (12:54-13:30 UT). By the analytic signal of each time-series constructed from the Morlet wavelet (Glassmeier, 1980; Hartinger et al., 2011), the phase difference between Bp and Ea remains to be ~90 degrees at 12:00-14:00 UT (period between two vertical purple lines) detected by THA in Figure 3n. The Poynting flux oscillates around zero in the radial direction and no time-averaged radial Poynting flux is detected during this interval. Additionally, compressional Bp and Ea components show enhanced power spectra of the discrete 0.8-1.5 mHz frequency at RA1 and RA2 in Figures 3k and 3m, demarked by two horizontal black dotted lines. The low power in this frequency range between the RA1 and RA2 interval is seemly in contrast with the constant frequency throughout the cavity predicted by the global mode resonance theory (e.g., Zhu & Kivelson, 1989; Samson et al., 1992a; Keiling et al., 2001; Waters et al., 2002). However, based on the temporary (~30 min) RA2-conjugated 1.4±0.5 mHz ground geomagnetic field disturbance in Figure 5c, we prefer to attribute this discrepancy to the rapidly evolving wave activities than THA approaching a stable node of radial fast mode. Nevertheless, these features at least indicate the existence of ~1.2 mHz radial standing wave resonance at different radial distances or during distinct periods of the dusk-sector magnetosphere.

Meanwhile, in Figures 3j, 3l, 3n and 3o, the toroidal waves including Ba and Er show the signature of FLR. We employ a Hilbert transform technique of the analytic signal to determine the instantaneous amplitude and phase of the individual wave (Glassmeier, 1980; Hartinger et al., 2011). At RA2, there is a 180-degree phase reversal of Er (blue curve) from $180^o$ to $0^o$ across the maximum of Ba amplitude envelope. Meanwhile, the polarization characteristics of the transverse component of the wave magnetic field, i.e., dBa versus dBr, in Figure 3o also switches from negative (-0.5) to positive (+0.2) across the region of maximum amplitude. Due to the disturbance of Er phase reversal, the cross-phase of Ba-Er (black curve) here also shifts from $-90^o$ (~13:00 UT) to $90^o$ (13:30-13:45 UT) across RA2, instead of keeping an expected stable standing mode structure at RA2 (e.g., Archer et al., 2022). This local toroidal wave amplification is also evident in the Ba power spectra at RA2 in Figure 3l. Based on our current space observations, we can prudently classify the phenomena at RA2 to be a potential candidate of the FLR (Southwood, 1974; Chen & Hasegawa, 1974a; Agapitov et al., 2009). Here we reasonably regard satellites to be near the null-point, considering that THA/THE travels near the magnetic equator ($<10^o$) and the asymmetric conductivity of north-south ionosphere usually slightly shifts the null-point away from the magnetic equator (Allan, 1982; Archer et al., 2021). The smoothed field-aligned

Poynting flux Sp in Figure 3r is northward at both RA1 and RA2, thus demonstrating the energy flow from FLR precipitating down to the north ionosphere. Certainly, abundant azimuthal energy flows including westward/sunward at RA1 and the eastward/antisunward at RA2 are also captured by THA, the direction reversal of which may result from the ~150$^{o}$ phase shift of compressional toroidal waves (Bp-Er; not shown here) from ~0$^{o}$ at RA1 to ~150$^{o}$ at RA2.

Applying the same analysis process to THE's observations in Figure 4, the major results and conclusion remain robust. However, several differences also appear: (1) Stronger compressional (Bp) component from Figure 4c; (2) The 90$^{o}$ cross-phase of radial standing wave is captured during a smaller period of 12:48-13:54 UT; (3) At RE2, the intensified toroidal wave roughly shows the signature of the undisturbed field-aligned standing waves (i.e., ~90$^{o}$ phase difference of Ba and Er), yet with no rapid phase jump of Er; (4) Southward Poynting fluxes are detected by THE in contrast with northward ones by THA. Consideration of the nearly same L-shell locations of two satellites at arbitrary times of 11:30-14:00 UT, one can mostly attribute these disparities to the effect of different MLT/MLAT between THA and THE, i.e., THE travelled closer to the dusk terminator/magnetic equator for approximate 0.8h/1-2$^{o}$ than THA. Nevertheless, the oscillations are generally very similar between the two spacecrafts, possibly suggests for the case of global standing mode waves.

Near four hours later, THD also swept across RA/E1 and RA/E2, detecting no field line resonance and radial standing wave within the expected frequency range (0.8-1.5 mHz), which is reasonable due to the rapidly evolving wave activities mentioned above.

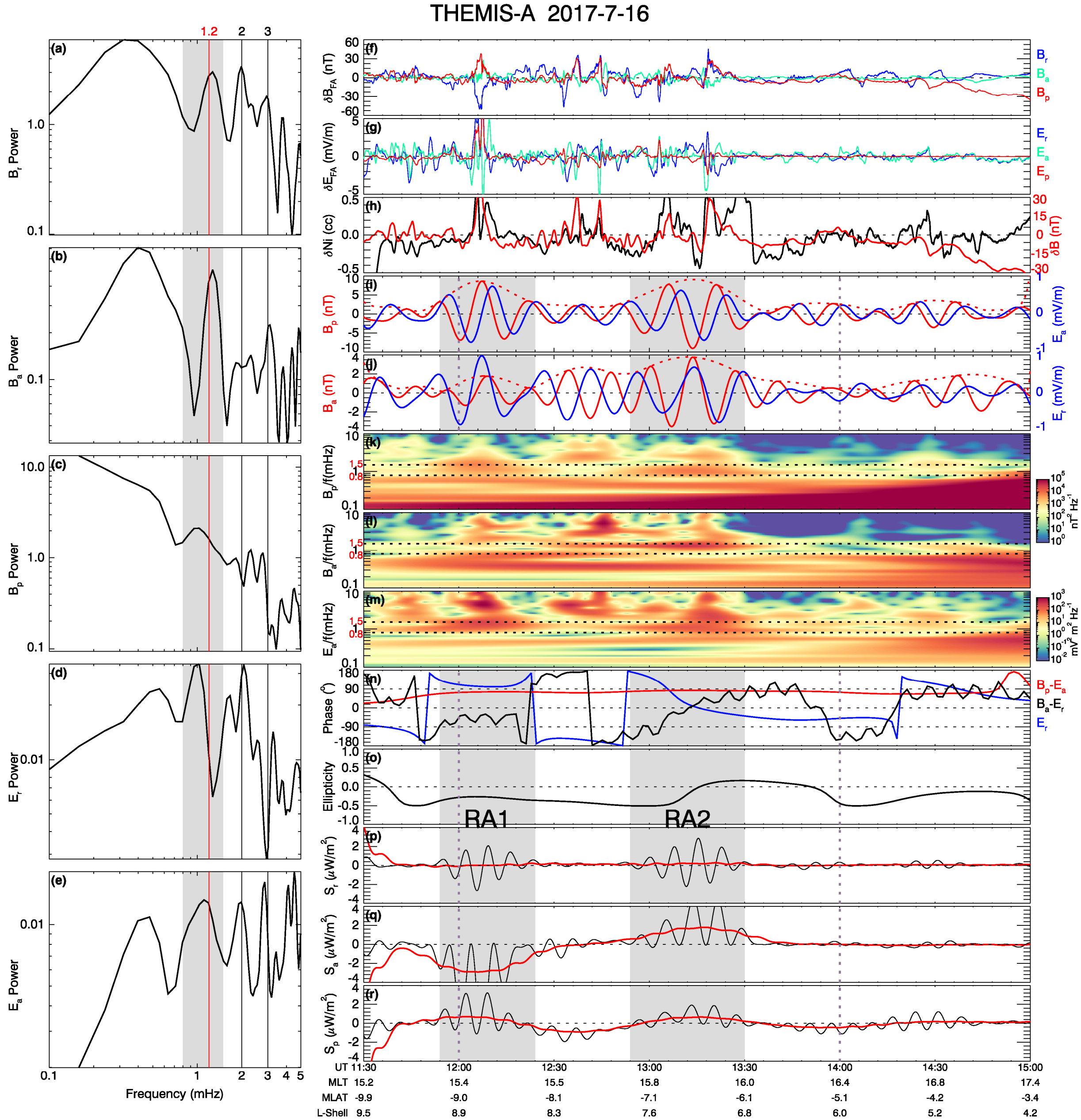


**Figure 3. Characteristics of Pc5 ULF waves measured by THA.** (a-e) power spectra of the magnetic and electric field perturbations in the field-aligned (FA) coordinate at 11:30-15:00 UT; (f-g) detrended (FA) magnetic and electric field; (h) ions number density (black) and B (red) perturbation; (i) Bandpass filtered (0.8-1.5 mHz) poleward Bp (red solid line), azimuthal Ea (blue solid line) and the envelop of Bp amplitude (red dotted line); (j) Bandpass filtered Ba, Er and the envelop of Ba amplitude; (k-m) Morlet wavelet dynamic power spectra of Bp, Ba and Ea; (n) Cross-phases of Bp-Ea (red) and Ba-Er (black) pairs and individual phase of Er (blue); (o) Polarization ellipse of the transverse wave, i.e., dBa versus dBr; (p-r) Raw (black) and smoothed (red; 30-min running boxcar) radial (Sr), azimuthal (Sa) and poleward (Sp) Poynting fluxes. Note that vertical lines in Figures 3a-3e demark the general power peaks of harmonic frequencies. The 0.8-1.5 mHz bandpass is highlighted by the gray shaded rectangle in Figures 3a-3e and two horizontal black dotted lines in Figures 3k-3m. While the gray shaded regions and vertical purple dotted lines in Figures 3i, 3j and 3n-3r are explained in the main text.

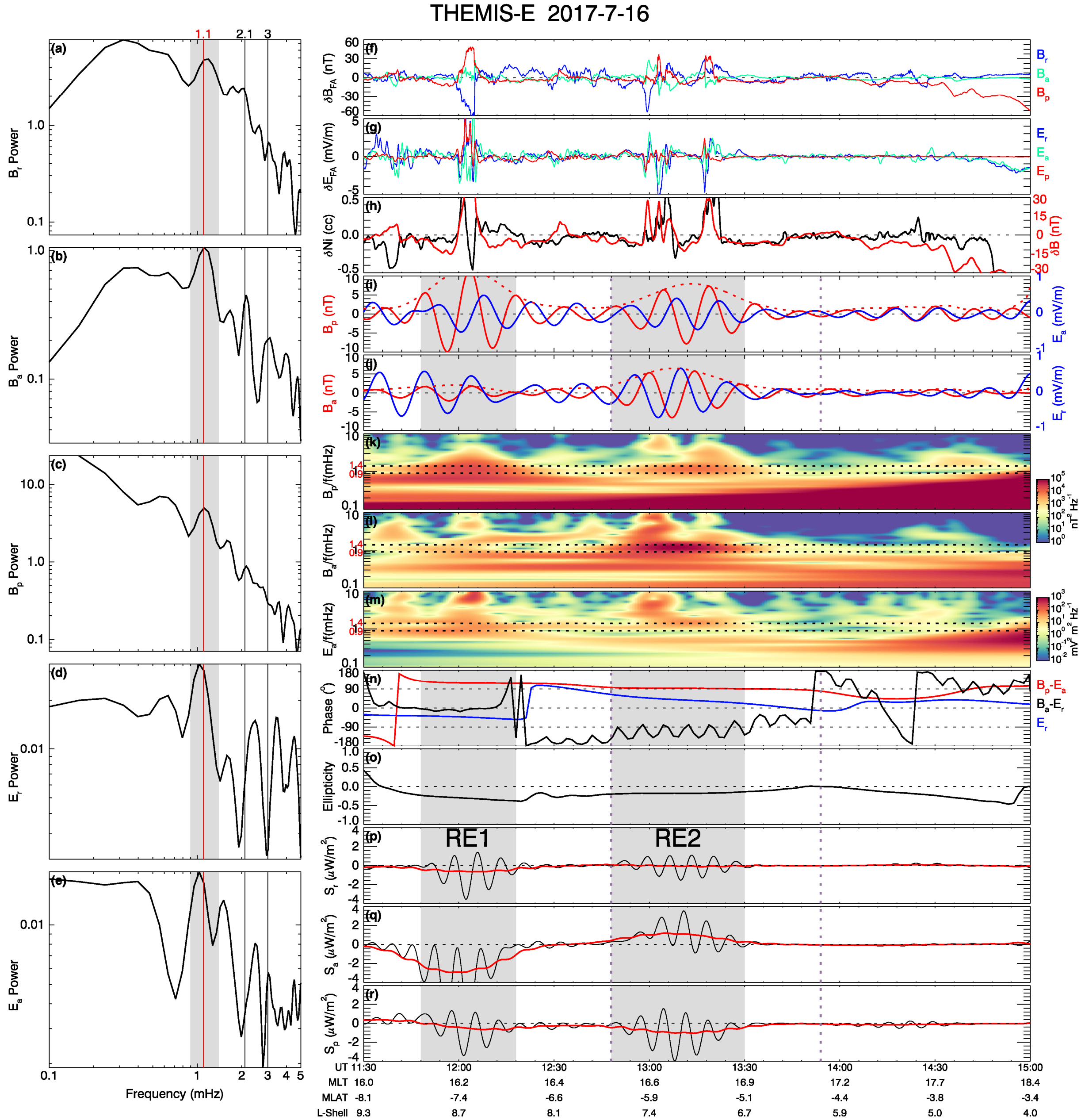


**Figure 4. Characteristics of Pc5 ULF waves measured by THE with similar layout as Figure 3**. Note there is a subtle displace between the 0.9-1.4 mHz bandpass filter centered at 1.1 mHz in Figure 4 (THE) and the 0.8-1.5 mHz bandpass filter centered at 1.2 mHz in Figure 3 (THA).

## 2.3 Ionosphere and Ground Observations

The conjugated ionospheric aurora and ground geomagnetic field disturbance are further demonstrated in Figure 5, overlapped by the footprints of THA and THE using the Tsyganenko 96 (T96) magnetic field model (Tsyganenko & Stern, 1996) and the geomagnetic field stations chain (blue dots). During 12:30-14:30 UT, these stations all detected 1.1 and 1.4 mHz horizontal and vertical geomagnetic field disturbances (He et al., 2020). The 1.4±0.5 mHz bandpass filter is utilized to construct the Figure 5c. Especially, SOR and MAS stations, just located at the conjugated footprint of the candidate FLR at RA/E2, display the similar FLR characteristics of the amplitude maximum at 13:00-13:40 UT, across which the phase of H-component (black) shifts by nearly 180º in Figure 5d (e.g., Samson et al., 1992a,b; Rae et al., 2005). The D-component (red) also has a comparable amplitude peak at MAS and MUO, accompanied by a ~180 phase reversal between MAS and SOR at 13:22 UT (blue vertical dotted line). On the other side, the aurora disk images in the north hemisphere in Figures 5a-5b is shot by the SSUSI onboard DMSP F18 and F17 satellites. Note that the aurora images of SSUSI are built-up from brushstroke-like scans across the Earth's disk and every scan lasts for 22 s. Near the SOR and MAS stations in Figures 5a and 5b, there occur evidently and locally enhanced aurora phenomena, whose luminosity is built up by F18 between 13:29 and 13:30 UT and by F17 between 13:31 and 13:32 UT. As expected, the ionospheric aurora brightening and ground FLR signatures match perfectly with the magnetospheric FLR characteristics at RA/E2 from both time and location aspects. Consequently, we may depict that the magnetospheric FLR can locally brighten ionospheric aurora and disturb geomagnetic field, possibly through the northward Poynting flux at RA2 in Figure 3r and southward ones at RE2 in Figure 4r if considering the energy reflection by the smooth southern ionosphere.

The similar intensified geomagnetic disturbance and enhanced ionospheric aurora were not observed near the conjugated region of RA/E1 (near BJN station), corresponding well with no evidence of strong FLR/toroidal fluctuations during the RA1 and RE1 intervals from Figures 3 and 4.. Interestingly, the evident giant undulations (GUs; e.g., Lui et al., 1982; Forsyth et al., 2020; Zhou et al. 2021, 2022) appear on the equator edge of diffuse aurora in Figures 5a and 5b, which are excited by the ~1.3 mHz plasmapause surface wave on the dusk-sector plasmapause, as firstly evidenced by He et al. (2020) in the same GUs event. Their potential relationship deserves a further investigation, based on the large GUs database established by Zhou et al. (2021, 2022).

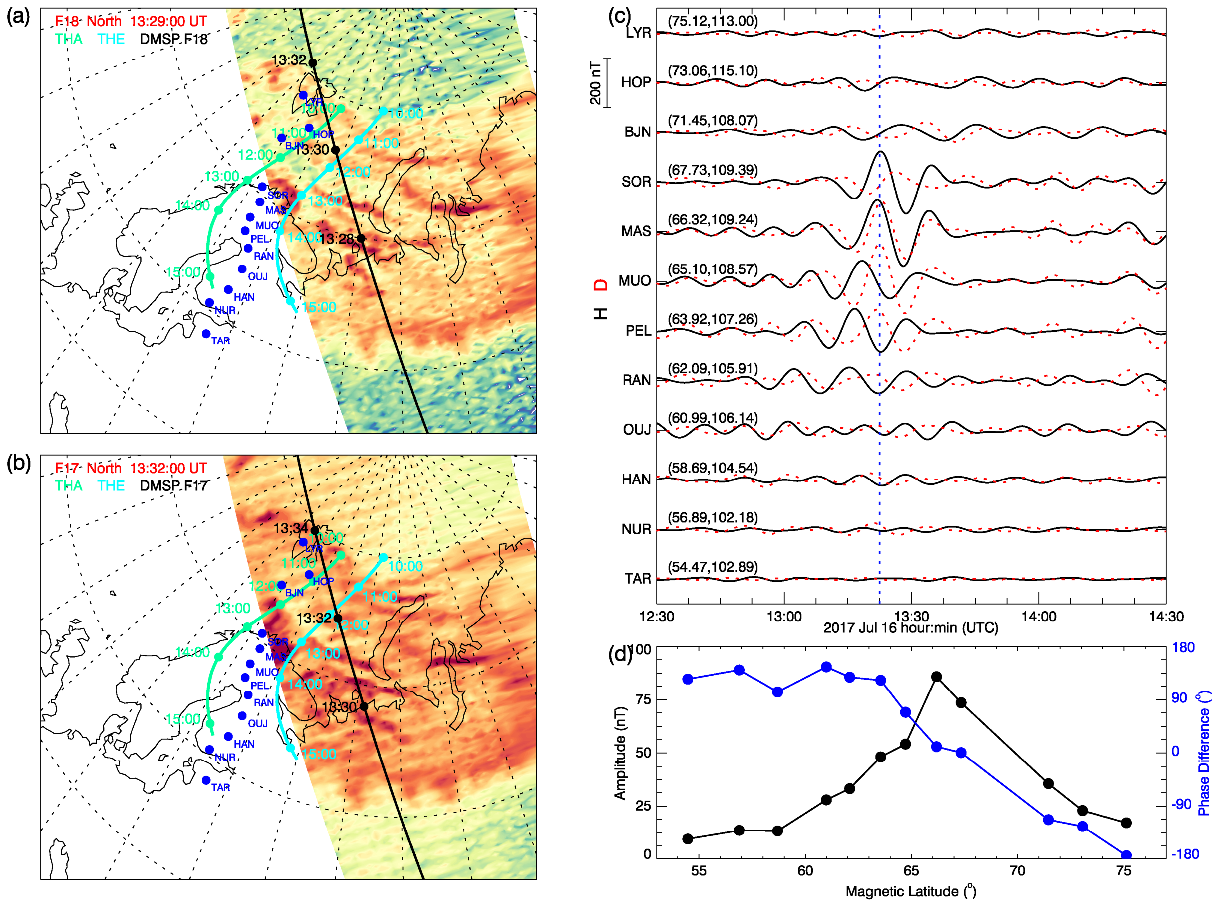


**Figure 5. Aurora and ground ULF waves.** (a-b) Station chain (blue dots) aligned in almost the same magnetic longitude in the IMAGE magnetometer array with the background northern auroral image concurrently observed by DMSP F18 and F17 satellites. The green, cyan and black curves trace the footprints of THA, THE and DMSP, individually. (c) Bandpass filtered (1.4±0.5 mHz) horizontal (H; black) and vertical (D; red) components of the geomagnetic field perturbations. The geomagnetic latitudes and longitudes of each station are shown above its curve. The blue vertical dotted line marks a time of phase reversal. (d) Amplitudes (black) and phase differences (blue) of the H component of the blue stations chain plotted as a function of geomagnetic latitudes.

## 3. Discussion and Conclusion

A radial standing Pc5-6 wave with the ~1.2 mHz discrete frequency is identified within the dusk-sector magnetosphere in this research, according to the inherent signatures of cavity modes derived from previous theoretical models and experimental research (e.g., Zhu & Kivelson, 1989; Samson et al., 1992; Waters et al., 2002; Takahashi et al., 2010, 2018). To roughly test whether the magnetosphere cavity can support such a low frequency, we further utilize the spacecraft potential inferred electron density (McFadden et al., 2008b) and measured magnetic field to calculate the general Alfvén velocity along the satellites' trajectories. We neglect spike values and average the Alfvén velocity tendency in the magnetosphere (4.2-8.9 L shells) to obtain the $\overline{v_A}$ ~410 km/s (THA) value, which is a reasonable approximation since there are small variations of the radial Alfvén velocity. The lowest possible fast mode resonance (FMR) frequency given by $f_{FMR}=\frac{\overline{v_A}}{4(R_{MP}-R_{PP})}$ (e.g., Mann et al., 1999) is roughly estimated to be ~2.2 mHz for a quarter wavelength mode between the MP ($R_{MP}$=11 $R_E$ obtained from the THD's MP crossing in Figure 1) and PP ($R_{PP}$=3.8 $R_E$ determined at the clear sharp electron density gradient measured by THE). Generally, this frequency is close to the 1.2 mHz frequency of observed radial standing wave signal when considering that the Alfvén velocity may be overestimated, especially serious near the PP, due to the cold protons and heavy ions composition. Regardless of the simple box model and the cursory estimation, the frequency matching at least provides a potential feasibility that the observed 1.2 mHz radial standing mode wave may be constructed between the sharp MP and PP in this case.

The sparsity of simultaneous space and ground observations of classical FLR is worthwhile to be noted (e.g., Southwood, 1974; Agapitov et al., 2009; Rae et al., 2005). And the shear and compressional MHD wave modes could couple via the FLR mechanism (e.g., Chen & Hasegawa, 1974b; Keiling et al., 2001; Hartinger et al., 2011). In this case, the essential characteristics of FLR are concurrently identified during the RA2 interval at the dusk-sector magnetosphere and conjugated ground location, in overlapping regions showing amplified standing wave. Combined with the northward Poynting flux and local aurora enhancement, we can obtain that the radial standing wave dissipates energy into upper atmosphere by coupling itself to the FLR, generating the visible local aurora enhancement within auroral oval. Certainly, the fast mode wave can also lose energy through the azimuthal Poynting flux, which shows it is azimuthally propagating instead of standing and therefore corresponds to a waveguide mode.

The crucial energy source supporting the Pc5-6 ULF wave in the magnetosphere deserves a further discussion. Solar wind is currently accepted to drive the magnetospheric ULF wave through the K-H instability/wave (e.g., Pu & Kivelson, 1983; Mann et al., 1999; Wright et al., 2000; Agapitov et al., 2009) and periodic fluctuations of the solar wind dynamic pressure (e.g., Kepko & Spence, 2003; Zong et al., 2007; Di Matteo et al., 2022) and impulse/shock (e.g., Mann et al., 1998; Takahashi et al., 2018). In this event, the magnetospheric dominant 1.2/1.1 mHz ULF waves observed by THA/THE at 11:30-13:30 UT plausibly correspond well with the discrete ~1 mHz magnetosheath ion dynamic pressure/velocity oscillation at 10:00-13:00 UT, possibly suggesting this radial standing wave and FLR in the flank magnetosphere may be triggered by the magnetosheath fluctuation outside the dusk-sector MP. Notably, this ~1 mHz magnetosheath fluctuation can be evidently identified by the dynamic pressure oscillation during 10:00-11:00 UT and is continuously reflected in the ion velocity oscillation due to a rapidly decreasing ion density during 11:30-13:30 UT. The latter seems to be unconspicuous in the dynamic power spectra, mostly overshadowed by the temporarily/locally more intense velocity distortion at 11:15-11:30 UT. Alternatively, the strong magnetosheath dynamic pressure oscillation at 10:00-11:00

UT likely have driven magnetospheric ULF waves to establish radial standing waves between MP and PP (e.g., Kepko & Spence, 2003; Zong et al., 2007). Then this magnetospheric radial standing wave might sustain for hours, consideration of a quasi-stable MP and PP locations, as determined from both the steady solar wind dynamic pressure and the nearly constant IMF Bz during 11:00-13:00 UT (Shue et al., 1998; He et al., 2017), and thus could be captured by THA and THE. Further, this magnetosheath fluctuation existing from 10:00 to 13:00 UT may originate from the solar wind based on their nearly the same dynamic pressure and density oscillation during 10:00-11:00 UT and the similar velocity fluctuation at 12:15-13:30 UT. Besides, internal instabilities triggered by the substorm energetic ion injection could also play a role at some point in the excitement of the ULF waves (e.g., Turner et al., 2015; Keiling et al., 2008). Yet this situation generally appears near the PP ($R_{PP}$=3.8 $R_E$), which is far away from the Pc5-6 ULF region (6.8-9 $R_E$) herein. In these regards, we suggest that the solar-wind/magnetosheath dynamic pressure and/or velocity fluctuations might be a reasonable driver for the observed radial standing waves.

The essential characteristics and effect of Pc5-6 (<2 mHz) ULF waves in the solar wind-magnetosphere-ionosphere coupled system are demonstrated and identified in this letter. Limited by the satellites' configuration, however, here we don't emphasize to distinguish the temporal evolving and spacial distribution effects of ULF waves, which could be resolved by multiple satellites in a string-of-pearls configuration combined with the self-consistent global MHD or hybrid models in the future. Nevertheless, our result in this letter would provide both physical insights and restrictions in improving the current global resonance model including the cavity mode and waveguide mode resonance and thus advance our understanding on the solar wind-magnetosphere-ionosphere energy coupling process.

**Acknowledgments**

This work was supported by the National Natural Science Foundation of China (42222408, 41931073), the National Key R&D Program of China (2021YFA0718600), the Youth Innovation Promotion Association of the Chinese Academy of Sciences (No. Y2021027), the Key Research Program of the Institute of Geology & Geophysics, Chinese Academy of Sciences (IGGCAS-201904) and the UKRI (STFC/EPSRC) Stephen Hawking Fellowship (EP/T01735X/1). We acknowledge NASA contract NAS5-02099 and V. Angelopoulos for use of data from the THEMIS Mission.

## Open Research

The THEMIS mission data are available at http://themis.ssl.berkeley.edu/data/themis/. The solar wind parameters are available from NASA OMNIWeb (https://omniweb.gsfc.nasa.gov/form/sc_merge_min1.html). The geomagnetic indices are available from World Data Center for geomagnetism, Kyoto at https://wdc.kugi.kyoto-u.ac.jp./wdc/Sec3.html. The IMAGE magnetometer data are available at https://space.fmi.fi/image/www/index.php?page=user_defined. The DMSP SSUSI data is available at https://ssusi.jhuapl.edu/data_availability. The IDL GEOPACK DLM used for the field line trace is available at https://ampere.jhuapl.edu/tools/. The SPEDAS software used for wave analysis is available at http://themis.ssl.berkeley.edu/software.shtml.

## References

Agapitov, O., Glassmeier, K. H., Plaschke, F., Auster, H. U. et al. (2009), Surface waves and field line resonances: A THEMIS case study. Journal of Geophysical Research, 114, A00C27. doi:10.1029/2008JA013553.

Allan, W. (1982), Phase variation of ULF pulsations along the geomagnetic field-line. Planetary and Space Science, 30(4), 339-346. doi:10.1016/0032-0633(82)90039-3.

Allan, W., White, S. P., & Poulter, E. M. (1986), Impulse-excited hydromagnetic cavity and field-line resonances in the magnetosphere. Planetary and Space Science, 34(4), 371-385. doi:10.1016/0032-0633(86)90144-3.

Angelopoulos, V. (2008), The THEMIS mission. Space Science Reviews, 141, 5-34, doi:10.1007/s11214-008-9336-1.

Archer, M. O., Hartinger, M. D., Walsh, B. M., Plaschke, F., & Angelopoulos, V. (2015), Frequency variability of standing Alfvén waves excited by fast mode resonances in the outer magnetosphere, Geophysical Research Letters, 42, 10,150-10,159, doi:10.1002/2015GL066683.

Archer, M. O., Hartinger, M. D., Walsh, B. M., & Angelopoulos, V. (2017), Magnetospheric and solar wind dependences of coupled fast-mode resonances outside the plasmasphere. Journal of Geophysical Research: Space Physics, 122, 212-226. doi:10.1002/2016JA023428.

Archer, M. O., Hietala, H., Hartinger, M. D., Plaschke, F., & Angelopoulos, V. (2019), Direct observations of a surface eigenmode of the dayside magnetopause. Nature Communications, 10, 615. doi:10.1038/s41467-018-08134-5.

Archer, M.O., Hartinger, M.D., Plaschke, F. et al. (2021), Magnetopause ripples going against the flow form azimuthally stationary surface waves. Nature Communications, 12, 5697. doi:10.1038/s41467-021-25923-7.

Archer, M. O., Southwood, D. J., Hartinger, M. D., Rastaetter, L., & Wright, A. N. (2022), How a realistic magnetosphere alters the polarizations of surface, fast magnetosonic, and Alfvén waves. Journal of Geophysical Research: Space Physics, 127, e2021JA030032. doi:10.1029/2021JA030032.

Auster, H. U., Glassmeier, K. H., Magnes, W., Aydogar, O., Baumjohann, W., Constantinescu, D., et al. (2008), The THEMIS Fluxgate Magnetometer. Space Science Reviews, 141, 235-264. doi:10.1007/s11214-008-9365-9.

Bonnell, J. W., Mozer, F. S., Delory, G. T., Hull, A. J., Ergun, R. E., et al. (2008), The Electric Field Instrument (EFI) for THEMIS. Space Science Reviews, 141, 303-341. doi:10.1007/s11214-008-9469-2.

Chen, L. & Hasegawa, A. (1974a), A theory of long-period magnetic pulsations: 1. Steady state excitation of field line resonance. Journal of Geophysical Research, 79(7), 1024-1032. doi:10.1029/JA079i007p01024.

Chen, L., & Hasegawa, A. (1974b), A theory of long-period magnetic pulsations: 2. Impulse excitation of surface eigenmode. Journal of Geophysical Research: Space Physics, 79(7), 1033-1037. doi:10.1029/ja079i007p01033.

Claudepierre, S. G., Elkington, S. R., & Wiltberger, M. (2008), Solar wind driving of magnetospheric ULF waves: Pulsations driven by velocity shear at the magnetopause. Journal of Geophysical Research, 113, A05218. doi:10.1029/2007JA012890.

Claudepierre, S. G., Wiltberger, M., Elkington, S. R., Lotko, W. & Hudson, M. K. (2009), Magnetospheric cavity modes driven by solar wind dynamic pressure fluctuations. Geophysical Research Letters, 36, L13101. doi:10.1029/2009GL039045.

Di Matteo, S., Villante, U., Viall, N., Kepko, L., & Wallace, S. (2022), On differentiating multiple types of ULF magnetospheric waves in response to solar wind periodic density structures. Journal of Geophysical Research: Space Physics, 127, e2021JA030144. doi:10.1029/2021JA030144.

Elkington, S. R. (2006), A review of ULF interactions with radiation belt electrons. in Magnetospheric ULF Waves: Synthesis and New Directions. Vol. 169 of Geophysical Monograph Series (eds. Takahashi, K., Chi, P. J. Denton, R. E. & Lysak, R. L.) 177-193 (John Wiley & Sons).

Elsden, T., & Wright, A. N. (2019), The effect of fast normal mode structure and magnetopause forcing on FLRs in a 3-D waveguide. Journal of Geophysical Research: Space Physics, 124, 178-196. doi:10.1029/2018JA026222.

Engebretson, M., Glassmeier, K.-H., Stellmacher, M., Hughes, W. J., & Lühr, H. (1998), The dependence of high-latitude Pc5 wave power on solar wind velocity and on the phase of high-speed solar wind streams. Journal of Geophysical Research, 103(A11), 26271-26283. doi:10.1029/97JA03143.

Eriksson, P. T. I., Blomberg, L. G., Schaefer, S., & Glassmeier, K. H. (2006), On the excitation of ULF waves by solar wind pressure enhancements. Annales Geophysicae, 24, 3161-3172. doi:10.5194/angeo-24-3161-2006.

Fenrich, F. R. & Waters, C. L. (2008), Phase coherence analysis of a field line resonance and solar wind oscillation. Geophys. Res. Lett., 35, L20102. doi:10.1029/2008GL035430.

Forsyth, C., Sergeev, V. A., Henderson, M. G. et al. (2020), Physical Processes of Meso-Scale, Dynamic Auroral Forms. Space Sci Rev, 216, 46. doi:10.1007/s11214-020-00665-y.

Glassmeier, K. H. (1980), Magnetometer array observations of a giant pulsation event. Journal of Geophysics, 48(3), 127-138.

Glassmeier, K.-H., Buchert, S., Motschmann, U., Korth, A., & Pedersen, A. (1999), Concerning the generation of geomagnetic giant pulsations by drift-bounce resonance ring current instabilities. Ann. Geophysicae, 17(3), 338-350. doi:10.1007/s00585-999-0338-4.

Golovchanskaya, I. V., Kornilov, I. A., Kornilova, T. A., Kornilov, O. I. & Kogai, T. G. (2018), Signatures of Alfvénic Field-Line Resonance in the Behavior of Preonset Auroral Arcs. Geomagnetism and Aeronomy, 58(1), 43-49. doi:10.1134/S0016793218010073.

Hartinger, M. D., Angelopoulos, V., Moldwin, M. B., Glassmeier, K.-H., & Nishimura, Y. (2011), Global energy transfer during a magnetospheric field line resonance. Geophysical Research Letters, 38, L12101. doi:10.1029/2011gl047846.

Hartinger, M. D., Turner, D. L., Plaschke, F., Angelopoulos, V., & Singer, H. (2013a), The role of transient ion foreshock phenomena in driving Pc5 ULF wave activity. Journal of Geophysical Research: Space Physics, 118(1), 299-312. doi:10.1029/2012JA018349.

Hartinger, M. D., Angelopoulos, V., Moldwin, M. B., Takahashi, K., & Clausen, L. B. N. (2013b), Statistical study of global modes outside the plasmasphere. Journal of Geophysical Research: Space Physics, 118, 804-822. doi:10.1002/jgra.50140.

He, F., Zhang, X.-X., Lin, R.-L., Fok, M.-C., Katus, R. M., Liemohn, M. W., Gallagher, D. L., & Nakano, S. (2017), A new solar wind-driven global dynamic plasmapause model: 2. Model and validation. Journal of Geophysical Research: Space Physics, 122, 7172-7187. doi:10.1002/2017JA023913.

He, F., Guo, R.-L., Dunn, W. R., Yao, Z.-H., Zhang, H. S., Hao, Y.-X., et al. (2020), Plasmapause surface wave oscillates the magnetosphere and diffuse aurora. Nature Communications, 11(1), 1668. doi:10.1038/s41467-020-15506-3.

Keiling, A., Wygant, J. R., Cattell, C., Kim, K.-H., Russell, C. T., Milling, D. K., et al. (2001), Pi2 pulsations observed with the Polar satellite and ground stations: Coupling of trapped and propagating fast mode waves to a midlatitude field line resonance. Journal of Geophysical Research: Space Physics, 106(A11), 25891-25904. doi:10.1029/2001ja900082.

Keiling, A., Angelopoulos, V., Larson, D., Lin, R., McFadden, J. et al. (2008), Correlation of substorm injections, auroral modulations, and ground Pi2. Geophys. Res. Lett., 35, L17S22. doi:10.1029/2008GL033969.

Keiling, A. (2009), Alfvén Waves and Their Roles in the Dynamics of the Earth's Magnetotail: A Review. Space Science Reviews, 142, 73-156. doi:10.1007/s11214-008-9463-8.

Keiling, A., Lee, D.-H. & Nakariakov, V. editors. (2016), Low-Frequency Waves in Space Plasmas. Geophysical Monograph Series (American Geophysical Union).

Kepko, L., & Spence, H. E. (2003), Observations of discrete, global magnetospheric oscillations directly driven by solar wind density variations. Journal of Geophysical Research, 108(A6), 1257. doi:10.1029/2002JA009676.

Kivelson, M. G., Etcheto, J. & Trotignon, J. G. (1984), Global compressional oscillations of the terrestrial magnetosphere: The evidence and a model. Journal of Geophysical Research, 89(A11), 9851-9856. doi:10.1029/ja089ia11p09851.

Kivelson, M. G., & Southwood, D. J. (1985), Resonant ULF waves: A new interpretation. Geophysical Research Letters, 12, 49-52. doi:10.1029/GL012i001p00049.

Kivelson, M. G., & Southwood, D. J. (1986), Coupling of global magnetospheric MHD eigenmodes to field line resonances. Journal of Geophysical Research: Space Physics, 91(A4), 4345-4351. doi:10.1029/ja091ia04p04345.

Kivelson, M. G., Cao, M., McPherron, R. L., & Walker, R. J. (1997), A possible signature of magnetic cavity mode oscillations in ISEE spacecraft observations. Journal of geomagnetism and geoelectricity, 49(9), 1079-1098.

Lee, D.-H., & Lysak, R. L. (1989), Magnetospheric ULF wave coupling in the dipole model: The impulsive excitation. Journal of Geophysical Research, 94(A12), 17097-17103. doi:10.1029/JA094iA12p17097.

Lee, D. H. (2006), MHD eigenmodes in the inner magnetosphere, in magnetospheric ULF waves: Synthesis and new directions (K. Takahashi, PJ Chi, RE Denton, & RL Lysak, Eds.). American Geophysical Union, Washington, DC. doi: 10.1029/169GM07.

Lin, R. P., Anderson, K. A., Ashford, S. et al. (1995), A three-dimensional plasma and energetic particle investigation for the wind spacecraft. Space Sci Rev, 71, 125-153. doi:10.1007/BF00751328.

Lin, Y., Johnson, J. R., & Wang, X. Y. (2010), Hybrid simulation of mode conversion at the magnetopause. Journal of Geophysical Research: Space Physics, 115, A04208. doi:10.1029/2009JA014524.

Lui, A. T. Y., Meng, C.-I., & Ismail, S. (1982), Large amplitude undulations on the equatorward boundary of the diffuse aurora. Journal of Geophysical Research, 87(A4), 2385-2400. doi:10.1029/ja087ia04p02385.

Mann, I. R., Wright, A. N., & Cally, P. S. (1995), Coupling of magnetospheric cavity modes to field line resonances: A study of resonance widths. Journal of Geophysical Research, 100(A10), 19441-19456. doi:10.1029/95JA00820.

Mann, I. R., Chisham, G., & Bale, S. D. (1998), Multisatellite and ground-based observations of a tailward propagating Pc5 magnetospheric waveguide mode. J. Geophys. Res., 103(A3), 4657-4669. doi:10.1029/97JA03175.

Mann, I. R., Wright, A. N., Mills, K. J., & Nakariakov, V. M. (1999), Excitation of magnetospheric waveguide modes by magnetosheath flows. Journal of Geophysical Research, 104(A1), 333-353. doi:10.1029/1998JA900026.

Mann, I. R., Voronkov, I., Dunlop, M., Donovan, E., Yeoman, T. K., et al. (2002), Coordinated ground-based and Cluster observations of large amplitude global magnetospheric oscillations during a fast solar wind speed interval. Annales Geophysicae, 20, 405-426. doi:10.5194/angeo-20-405-2002.

McFadden, J. P., Carlson, C. W., Larson, D., Angelopoulos, V., Ludlam, M., Abiad, R., et al. (2008a), The THEMIS ESA plasma instrument and in-flight calibration. Space Science Reviews. doi:10.1007/s11214-008-9440-2.

McFadden, J. P., Carlson, C. W., Larson, D., Bonnell, J., Mozer, F., Angelopoulos, V., et al. (2008b), THEMIS ESA first science results and performance issues. Space Science Reviews. doi:10.1007/s11214-008-9433-1.

Mills, K. J., & Wright, A. N. (1999), Azimuthal phase speeds of field line resonances driven by Kelvin-Helmholtz unstable waveguide modes. Journal of Geophysical Research, 104(A10), 22667-22677. doi:10.1029/1999JA900280.

Motoba, T., Kikuchi, T., Okuzawa, T., & Yumoto, K. (2003), Dynamical response of the magnetosphere-ionosphere system to a solar wind dynamic pressure oscillation. J. Geophys. Res., 108(A5), 1206. doi:10.1029/2002JA009696.

Nishida, A. (2013), Geomagnetic diagnosis of the magnetosphere. (Vol. 9). Springer Science & Business Media.

Paxton, L. J., Morrison, D., Zhang, Y. L., Kil, H., Wolven, B., Ogorzalek, B. S., et al. (2002), Validation of remote sensing products produced by the special sensor ultraviolet scanning imager (SSUSI): a far UV-imaging spectrograph on DMSPF-16. Proc. SPIE 4485, 338-348. doi:10.1117/12.454268.

Piersanti, M., Di Matteo, S., Zhima, Z., Yang, Y., Zhang, Z., Marcucci, M. F., et al. (2022), On the source of the anomalous ULF waves detected at both ground and space-borne data on 23 June 2020. Journal of Geophysical Research: Space Physics, 127, e2021JA030044. doi:10.1029/2021JA030044.

Pu, Z.-Y. & Kivelson, M. G. (1983), Kelvin-Helmholtz instability at the magnetopause: Solution for compressible plasmas. Journal of Geophysical Research, 88(A2), 841-852. doi:10.1029/ja088ia02p00841.

Rae, I. J., Donovan, E. F., Mann, I. R., Fenrich, F. R., Watt, C. E. J., Milling, D. K., et al. (2005), Evolution and characteristics of global Pc5 ULF waves during a high solar wind speed interval. Journal of Geophysical Research, 110, A12211. doi:10.1029/2005ja011007.

Rae, I. J., Watt, C. E. J., Fenrich, F. R., Mann, I. R., Ozeke, L. G. & Kale, A. (2007), Energy deposition in the ionosphere through a global field line resonance. Annales Geophysicae, 25(12), 2529-2539. doi:10.5194/angeo-25-2529-2007.

Rickard, G. J., & Wright, A. N. (1994), Alfvén resonance excitation and fast wave propagation in magnetospheric waveguides. Journal of Geophysical Research, 99(A7), 13455-13464. doi:10.1029/94JA00674.

Samson, J. C., Jacobs, J. A. & Rostoker, G. (1971), Latitude-dependent characteristics of long-period geomagnetic micropulsations. Journal of Geophysical Research, 76(16), 3675-3683. doi:10.1029/ja076i016p03675.

Samson, J. C., Harrold, B. G., Ruohoniemi, J. M., Greenwald, R. A., & Walker, A. D. M. (1992a), Field line resonances associated with MHD wave guides in the magnetosphere. Geophysical Research Letters, 19, 441-444. doi:10.1029/92GL00116.

Samson, J. C., Wallis, D. D., Hughes, T. J., Creutzberg, F., Ruohoniemi, J. M. & Greenwald, R. A. (1992b), Substorm intensifications and field line resonances in the nightside magnetosphere. Journal of Geophysical Research, 97(A6), 8495-8518. doi:10.1029/91ja03156.

Shue, J.-H., Song, P., Russell, C. T., et al. (1998), Magnetopause location under extreme solar wind conditions. Journal of Geophysical Research, 103(A8), 17691-17700. doi:10.1029/98JA01103.

Southwood, D. J. (1974), Some features of field line resonances in the magnetosphere. Planetary and Space Science, 22(3), 481-491. doi:10.1016/0032-0633(74)90078-6.

Stephenson, J. A. & Walker, A. D. M. (2002), HF radar observations of Pc5 ULF pulsations driven by the solar wind. Geophys. Res. Lett., 29(9). doi:10.1029/2001GL014291.

Summers, D., Mann, I. R., Baker, D. N. & Schulz, M. editors. (2013), in Dynamics of the Earth's Radiation Belts and Inner Magnetosphere. Vol. 199 of Geophysical Monograph Series (American Geophysical Union).

Takahashi, K., Bonnell, J., Glassmeier, K-H., Angelopoulos, V., Singer, H. J., Chi, P. J., et al. (2010), Multipoint observation of fast mode waves trapped in the dayside plasmasphere. Journal of Geophysical Research, 115, A12247. doi:10.1029/2010JA015956.

Takahashi, K., Lysak, R., Vellante, M., Kletzing, C. A., Hartinger, M. D., & Smith, C. W. (2018), Observation and numerical simulation of cavity mode oscillations excited by an interplanetary shock. Journal of Geophysical Research: Space Physics, 123, 1969-1988. doi:10.1002/2017JA024639.

Tanskanen, E. I. (2009), A comprehensive high-throughput analysis of substorms observed by IMAGE magnetometer network: Years 1993-2003 examined. Journal of Geophysical Research, 114, A05204. doi:10.1029/2008ja013682.

Tsyganenko, N. A. & Stern, D. P. (1996), Modeling the global magnetic field of the large-scale Birkeland current systems. Journal of Geophysical Research, 101(A12), 27187-27198. doi:10.1029/96ja02735.

Turner, D. L., Claudepierre, S. G., Fennell, J. F., O'Brien, T. P., Blake, J. B., Lemon, C., Gkioulidou, M., et al. (2015), Energetic electron injections deep into the inner magnetosphere associated with substorm activity. Geophys. Res. Lett., 42, 2079-2087. doi: 10.1002/2015GL063225.

Walker, A. D. M., Ruohoniemi, J. M., Baker, K. B., Greenwald, R. A., & Samson, J. C.. (1992), Spatial and temporal behavior of ULF pulsations observed by the Goose Bay HF radar. Journal of Geophysical Research, 97, 12,187-12,202. doi:10.1029/92JA00329.

Wang, B., Liu, T., Nishimura, Y., Zhang, H., Hartinger, M., Shi, X., et al. (2020), Global propagation of magnetospheric Pc5 ULF waves driven by foreshock transients. Journal of Geophysical Research: Space Physics, 125, e2020JA028411. doi:10.1029/2020JA028411.

Waters, C. L., Takahashi, K., Lee, D.-H., & Anderson, B. J. (2002), Detection of ultralow-frequency cavity modes using spacecraft data. Journal of Geophysical Research, 107(A10), 1284. doi:10.1029/2001JA000224.

Wright, A. N. (1994), Dispersion and wave coupling in inhomogeneous MHD waveguides. Journal of Geophysical Research, 99(A1), 159-167. doi:10.1029/93JA02206.

Wright, A. N., Mills, K. J., Ruderman, M. S., & Brevdo, L. (2000), The absolute and convective instability of the magnetospheric flanks. Journal of Geophysical Research, 105(A1), 385-393. doi:10.1029/1999JA900417.

Yamakawa, T., Seki, K., Amano, T., Miyoshi, Y., Takahashi, N., Nakamizo, A., & Yamamoto, K. (2022), Excitation of two types of storm-time Pc5 ULF waves by ring current ions based on the magnetosphere-ionosphere coupled model. Journal of Geophysical Research: Space Physics, 127, e2022JA030486. doi:10.1029/2022JA030486.

Zhang, X. X., He, F., Lin, R. L., Fok, M. C., Katus, R. M., Liemohn, M. W., et al. (2017), A new solar wind driven global dynamic plasmapause model: 1. Database and Statistics: Plasmapause location database. Journal of Geophysical Research: Space Physics, 122(7), 7153-7171. doi:10.1002/2017JA023912.

Zhou, Y.-J., He, F., Zhang, X.-X., Yao, Z.-H., Wei, Y., & Zhang, Y.-L. (2021), Statistical characteristics of giant undulations during geomagnetic storms. Geophysical Research Letters, 48, e2021GL093098. doi:10.1029/2021GL093098.

Zhou, Y.-J., He, F., Yao, Z.-H., Wei, Y., Zhang, X.-X., & Zhang, Y.-L. (2022), Correlations between giant undulations and plasmapause configurations. Geophysical Research Letters, 49, e2022GL098627. doi:10.1029/2022GL098627.

Zhu, X., & Kivelson, M. G. (1989), Global mode ULF pulsations in a magnetosphere with a nonmonotonic Alfvén velocity profile. Journal of Geophysical Research, 94(A2), 1479-1485. doi:10.1029/JA094iA02p01479.

Zong, Q.-G., Zhou, X.-Z., Li, X., Song, P., Fu, S. Y., Baker, D. N., et al. (2007), Ultralow frequency modulation of energetic particles in the dayside magnetosphere. Geophysical Research Letters, 34, L12105. doi:10.1029/2007GL029915.